*Bull. Mater. Sci.* (2019) 42:239
https://doi.org/10.1007/s12034-019-1920-3


# Photodegradation of methylene blue over a new down-shifting luminescence catalyst

**RUI LIU[1,2], TAO LIU[2], YINGJIE QIAO[1,*], YONGCHAO BIE[2] and YINGJIN SONG[2]**
[1]College of Materials Science and Chemical Engineering, Harbin Engineering University, Harbin 150001, People's Republic of China
[2]Drug Engineering Research Centre, Harbin University of Commerce, Harbin 150076, People's Republic of China
*Author for correspondence (qiaoyingjie@hrbeu.edu.cn)

MS received 10 January 2019; accepted 25 April 2019

**Abstract.** $TiO_2$ nanotube arrays prepared by anodization technology are modified with a samarium ion ($Sm^{3+}$) by a hydrothermal method for use in photodegradation of methylene blue (MB). The samarium ion as a down-shifting luminescence material can improve UV radiation harvesting to increase visible light utilization. The efficiency of the photocatalytic activity for the modified-$TiO_2$ nanotube arrays in degradation of MB was investigated under UV–Vis light irradiation. The results show that Sm–$TiO_2$ nanotubes can increase the photocatalytic efficiency of MB. When $TiO_2$ nanotubes are modified by 0.02 M $Sm^{3+}$, MB can be almost completely degraded when compared with bare $TiO_2$ nanotubes. This indicates that $TiO_2$ nanotubes structure, surface area and good UV radiation harvesting play important roles in the degradation of MB.

**Keywords.** $TiO_2$ nanotube arrays; photodegradation; samarium ion; down-shifting material.

## 1. Introduction

Grätzel and O'Reagan [1–3] proposed one-dimensional $TiO_2$ nanotube arrays synthesized by an anodized-oxidation method. Because of their high-specific surface area, unique electrical properties, electron lifetime and electron transport [4,5], they were used in many areas, such as dye-sensitized solar cells [6,7], photocatalysts [8,9] and adsorption properties [10,11]. Many researchers are interested in the photocatalytic performance of $TiO_2$nanotube arrays. Yu *et al* [12] prepared new plasmonic photocatalyst Ag/AgCl/$TiO_2$ nanotube arrays by depositing AgCl nanoparticles, which exhibit a highly visible-light photocatalytic mechanism. Song *et al* [13] synthesized graphene and $TiO_2$ nanotube array composites by assembling graphene oxide (GO) on the surface of self-organized $TiO_2$ nanotube arrays through a simple impregnation method. The composites were enhanced by about 15 times for maximum photoconversion efficiency. The results presented GO to be efficient for the improved utilization of visible light for $TiO_2$ nanotube arrays. Liu *et al* [6] have fabricated nanotube arrays of different lengths to investigate the effects of the array lengths on the efficiency of $TiO_2$ nanotube arrays. However, many researches have neglected low-light harvesting of $TiO_2$ nanotube arrays. If most of the light can be transformed to visible light by a down-shifting luminescence material [14–17], more irradiation will be absorbed to improve light harvesting. Lanthanide-derived compounds have widely been used as efficient light conversion materials due to their specific 4f electronic structure and unique structure [18,19]. Samarium ions ($Sm^{3+}$) in the lanthanide ions have been considered as the most efficient down-shifting material, which can absorb ultraviolet light to visible light [20–23].

In this paper, we report highly ordered $TiO_2$ nanotube arrays fabricated on Ti sheets, which are modified by samarium ions ($Sm^{3+}$) by a hydrothermal method for use in the photodegradation of methylene blue (MB). We have investigated the properties and performance of different concentrations of Sm–$TiO_2$ nanotubes to increase the absorption of visible light and the efficiency. Moreover, the mechanism of degradation was also discussed.

## 2. Experimental

### 2.1 *Preparation of Sm–$TiO_2$ nanotubes*

$TiO_2$nanotube arrays were fabricated using an anodization method at 40 V for 6 h through magnetic stirring, as previously reported [24]. The electrolyte contained ethylene glycol, 0.3 wt% $NH_4F$ and 2 vol% water. The $TiO_2$ nanotube arrays were calcined at 500°C for 2 h. Sm–$TiO_2$ nanotubes were prepared by a hydrothermal method. The $TiO_2$ nanotube arrays were put into 0.01, 0.02, 0.03 and 0.05 M $Sm(NO_3)_3$ solutions, respectively. All the samples were heated to 120°C for 10 h in a drying oven. Finally, they were annealed at 500°C in a furnace for 1 h.

Published online: 23 July 2019

### 2.2 *Characterization*

Dimension-P2 Raman spectroscopy was used to measure Raman shifts. A micromeritics, ASAP 2101 was used for Brunauer–Emmett–Teller (BET) analysis. The morphology was observed with a field-emission scanning electron microscopy (FESEM, JEOL JSM-7401F) at 5 kV and an amplification ratio of 50,000. Photoluminescence (PL) spectra were analysed using a fluorescence spectrometer (F-4500). Ultraviolet–visible (UV–Vis) diffuse reflection spectra of the samples were recorded with a UV–Vis 2550 spectrophotometer.

### 2.3 *Photocatalytic degradation of MB*

Photocatalytic degradation of MB ($C_{16}H_{18}ClN_3S$) was irradiated by UV light, in which a 6 W, 255 nm UV lamp was used as the light source. Then, both the MB and catalyst were put into a homemade reactor. The duration of the UV irradiation time was 2 h. The samples were centrifuged at 3000 rpm for 10 min to separate the solid and liquid phases from the mixture solution. After centrifugation, the remaining concentration of MB in the solution was measured by a UV–Vis spectrophotometer at 699 nm.

## 3. Results and discussion

Figure 1a shows the highly ordered $TiO_2$ nanotube arrays with 100 nm diameter. The inset of figure 1a shows a tube structure with a length of 12 μm. Similar images were observed for different concentrations of Sm–$TiO_2$ nanotubes as shown in figure 1b–d. The tubular structure changed little. For 0.05 M Sm–$TiO_2$ nanotubes, a large amount of floccus appeared on the surface (figure 1e).

Figure 2A shows the Raman spectrum of $TiO_2$ nanotubes and different concentrations of Sm–$TiO_2$ nanotubes. Raman spectroscopy can determine the crystal structure, crystallinity and phase transition. The full width at half maximum of the peak is related to the position and grain size of the Raman peak [25]. According to group theory, the anatase phase has six active Raman peaks ($A_{1g}$+2$B_{1g}$+3$_{Eg}$), including 144 ($E_g$), 197 ($E_g$), 639 ($E_g$), 513 ($A_{1g}$), 400 ($B_{1g}$) and 519 $cm^{-1}$ ($B_{1g}$) [26]. Pure $TiO_2$ nanotube arrays are anatase phase crystals. The characteristic peaks of Sm–$TiO_2$ nanotubes are similar to those of pure $TiO_2$ nanotubes, which indicate that $Sm^{3+}$ modification does not change the crystal phase of the $TiO_2$ nanotube arrays. However, the intensity of the diffraction peak was decreased after $Sm^{3+}$ modification. The peak intensity decreased with an increase in the $Sm^{3+}$ concentration. This is due to the perturbation caused by the entry of $Sm^{3+}$ into the lattice gap, which will have a destructive effect on the symmetry of translation crystal. To a further observation, figure 2B shows a magnified view of the peak at 144 $cm^{-1}$ of the pure $TiO_2$ nanotube arrays and different concentrations of Sm–$TiO_2$ nanotubes. For the peak at 144 $cm^{-1}$, the half-height of the peak broadens slightly with an increase in the $Sm^{3+}$ concentration, which is attributed to the decrease in the grain size. As the grain size decreases, the interatomic distance decreases, leading to an increase in the force constant, a volume shrinkage effect and a vibration property of the material.

The BET results are given in table 1. It was observed that the specific surface area of the samples increases with

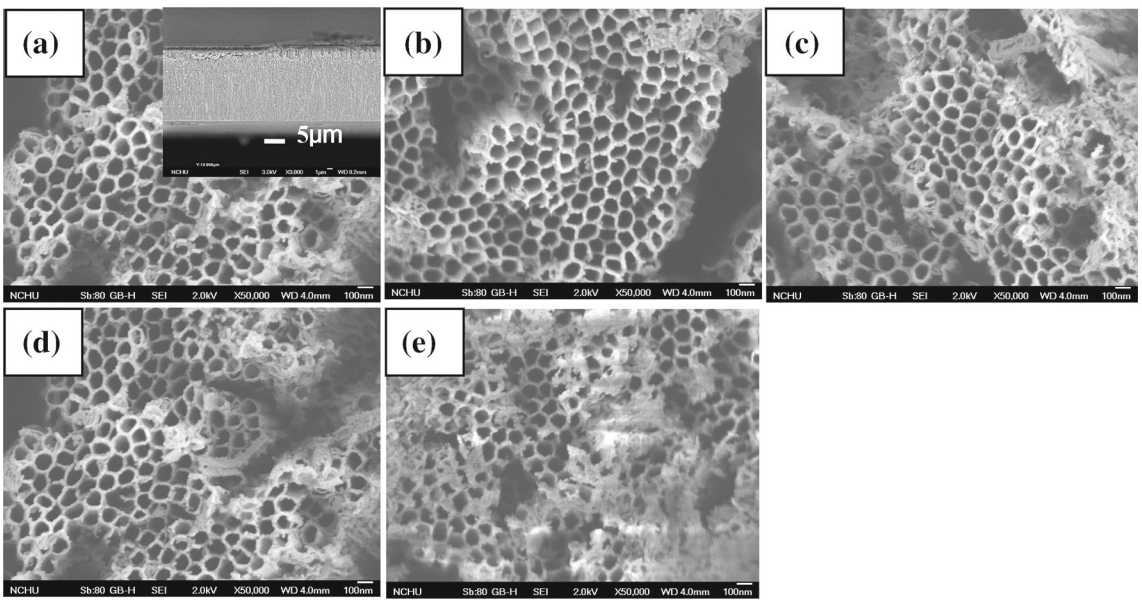


**Figure 1.** FESEM micrographs of $TiO_2$ nanotubes and Sm–$TiO_2$ nanotubes: (**a**) $TiO_2$ nanotubes, (**b**) 0.01, (**c**) 0.02, (**d**) 0.03 and (**e**) 0.05 M Sm–$TiO_2$ nanotubes.

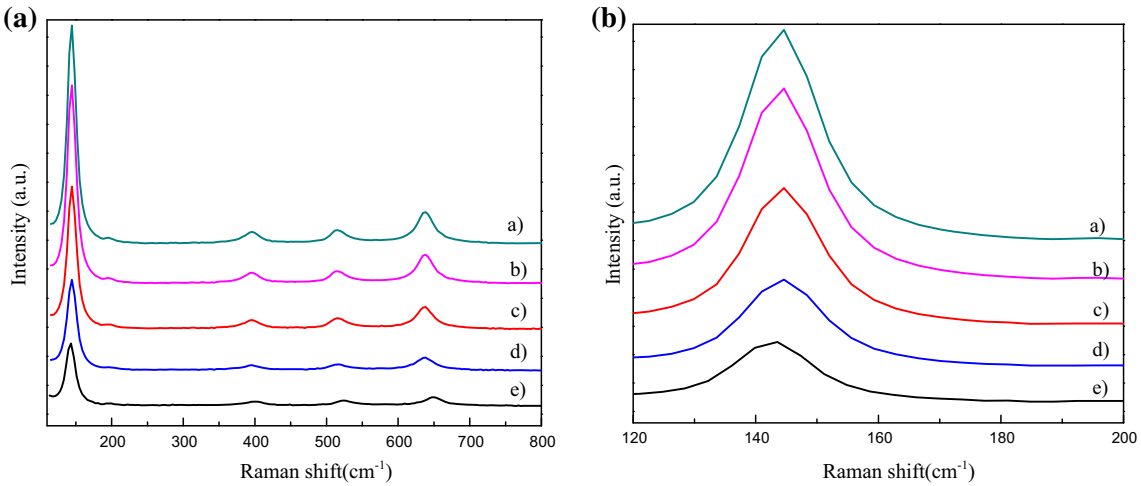


**Figure 2.** (**A**) Raman spectrum of $TiO_2$ nanotubes and different concentrations of Sm–$TiO_2$ nanotubes. (**B**) Enlarged Raman spectrum: (a) $TiO_2$ nanotubes, (b) 0.01, (c) 0.02, (d) 0.03 and (e) 0.05 M Sm–$TiO_2$ nanotubes.

**Table 1.** Surface area and pore volume of $TiO_2$ nanotubes and $Sm_2O_3/TiO_2$ nanotubes.

| Samples | $S_{BET}$ ($m^2\ g^{-1}$) | Pore volume ($cm^3\ g^{-1}$) |
|---|---|---|
| $TiO_2$ nanotubes | 90.0 | 0.09 |
| 0.01 mol $l^{-1}$ $Sm_2O_3/TiO_2$ nanotubes | 155.7 | 0.28 |
| 0.02 mol $l^{-1}$ $Sm_2O_3/TiO_2$ nanotubes | 316.8 | 0.43 |
| 0.03 mol $l^{-1}$ $Sm_2O_3/TiO_2$ nanotubes | 289.6 | 0.39 |
| 0.05 mol $l^{-1}$ $Sm_2O_3/TiO_2$ nanotubes | 188.1 | 0.25 |

$Sm^{3+}$ concentration up to 0.02 M, where 0.02 M Sm–$TiO_2$ nanotubes have the highest surface area with 316.8 $m^2\ g^{-1}$. This indicates that an appropriate concentration of $Sm^{3+}$ governs the particle size. At higher concentration above 0.03 M, both the surface area and pore volume are decreased. In contrast, for pure $TiO_2$ nanotube arrays, the specific surface area and pore volume are 90 and 0.09, respectively.

Figure 3 presents X-ray photoelectron spectroscopy (XPS) spectra of 0.02 M Sm–$TiO_2$ nanotubes. In the full spectrum of 0.02 M Sm–$TiO_2$ nanotubes as shown in figure 3a, the C element is derived from trace organics in the test equipment. Modified nanotube arrays contain Ti, O and Sm elements, as shown in table 2. The atomic percentage content of Sm increases with an increase in the concentration from 0.01 to 0.05 M Sm–$TiO_2$ nanotubes. Figure 3b shows high-resolution XPS spectra of O1s for 0.02 M Sm–$TiO_2$ nanotubes. From the figure, we can see that pure $TiO_2$ nanotube arrays have very good O 1s symmetry peaks, which indicate that O has only one existence state in this case. While asymmetric peaks appear in the Sm–$TiO_2$ nanotubes, they indicate that O also exists in a chemical state. Asymmetric oxygen peaks are divided into two peaks of 529.69 and 531.06 eV using XPS Peak software as shown in the inset diagram, showing oxygen atoms assigned to $TiO_2$ and $Sm_2O_3$, respectively. Figure 3c shows high-resolution XPS spectra of Ti2p for 0.02 M Sm–$TiO_2$ nanotubes. The two characteristic peaks of pure $TiO_2$ nanotube arrays at 459.3 and 465 eV are attributed to $Ti^{4+}(2p_{3/2})$ and $Ti^{4+}(2p_{1/2})$, respectively, indicating that the chemical state of Ti is $Ti^{4+}$. Compared to $TiO_2$ nanotube arrays, the characteristic peak of Sm–$TiO_2$ nanotubes moves towards low energy, and similar displacements can also be observed in the O1s spectrum. This is because the introduction of Sm forms Sm–O–Ti bonds on the surface of $TiO_2$, which affects the chemical environment surrounding $Ti^{4+}$, and density of electron clouds also decreases. Figure 3d shows high-resolution XPS spectra of Sm 3d for 0.02 M Sm–$TiO_2$ nanotubes. The two distinct peaks at 1083.6 and 1110.4 eV are Sm $3d_{5/2}$ and Sm $3d_{3/2}$, respectively, confirming that Sm is presented in a trivalent form.

Figure 4A shows UV–Vis diffuse reflectance spectroscopy (DRS) spectra of $TiO_2$ nanotube arrays and different concentrations of Sm–$TiO_2$ nanotubes. Pure $TiO_2$ nanotube arrays have a strong absorption band edge at 380 nm. This band is formed by the electron transition from the O 2p to the Ti 3d orbital. The absorption band moves towards the direction of high wavenumber after $Sm^{3+}$ modification. Moreover, the degree of the red-shift increases as the concentration of $Sm^{3+}$ increases. On the one hand, this may be due to an electron transfer from the 2p orbital of $O^{2-}$ to the 4f orbital of $Sm^{3+}$, which transfers energy to the $TiO_2$ nanotube arrays. On the

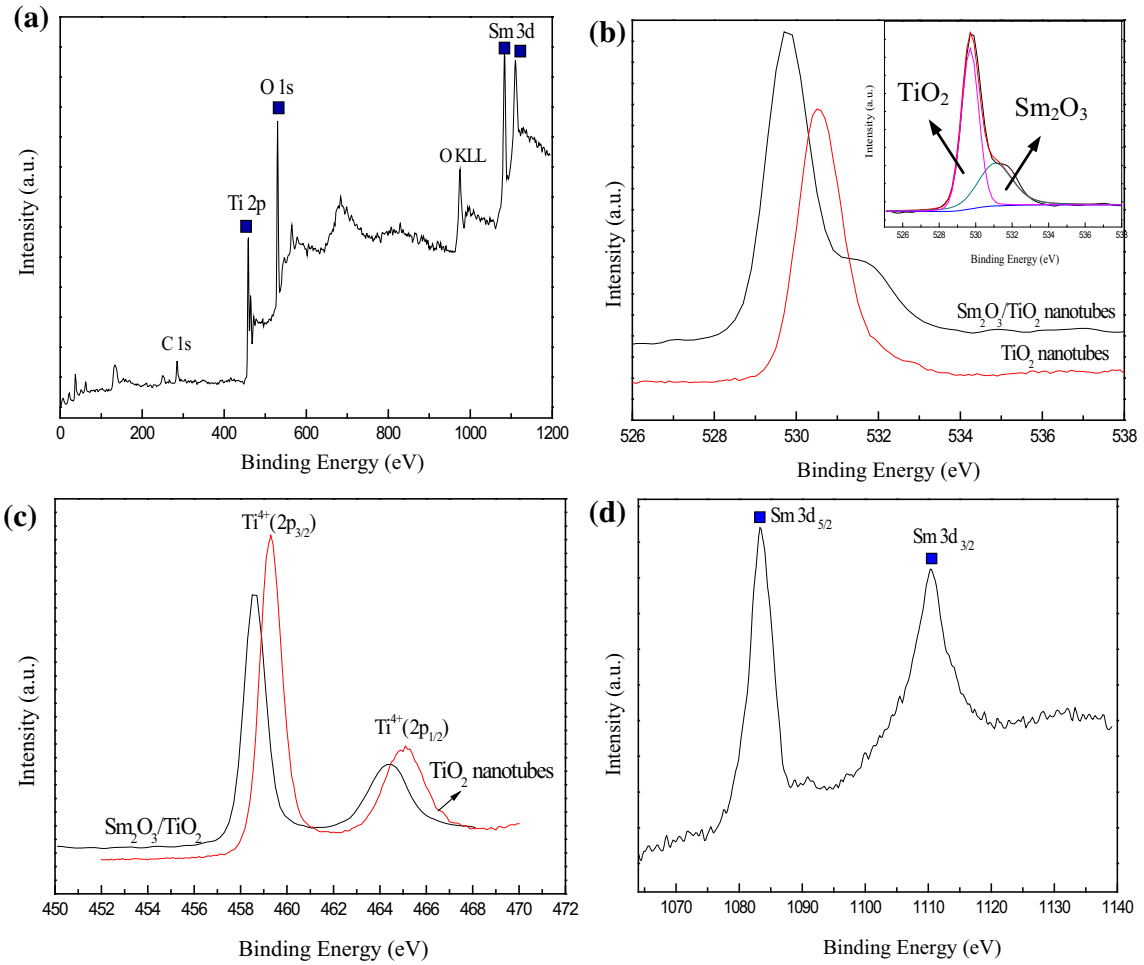


**Figure 3.** XPS spectrum of $TiO_2$ nanotubes and 0.02 M Sm–$TiO_2$ nanotubes: (**a**) survey spectra, (**b**) O 1s, (**c**) Ti 2p and (**d**) Sm 3d.

other hand, the introduction of $Sm^{3+}$ can change the energy level structure of $TiO_2$ nanotube arrays and forms a new energy level. The new energy level can accept excited electrons in the valence band of $TiO_2$, so that the photon of small energy is excited to a new energy level to capture electrons, resulting in the red-shift of the absorption edge. It can be seen that the introduction of $Sm^{3+}$ can extend the light absorption range, expands the visible light response range and improves the utilization of light. The width of the forbidden band can be calculated according to equation (1) with $h\upsilon$ as abscissa and $(\alpha h\upsilon)^2$ as the ordinate, in which the intercept of the extrapolation is the band gap, as shown in figure 4B.

$$\alpha = \frac{(h\upsilon - E_g)^{1/2}}{h\upsilon}. \quad (1)$$

The calculated band gap of the pure $TiO_2$ nanotube arrays is 3.26 eV. The band gap is 3.25, 3.07, 3.05 and 2.99 eV, respectively, for 0.01, 0.02, 0.03 and 0.05 M Sm–$TiO_2$ nanotubes. There is almost no change in the band gap after 0.01 M $Sm^{3+}$-modified $TiO_2$ nanotubes, indicating that the added amount is too small to change the band gap width. As the concentration of $Sm^{3+}$ increases, the band gap moves to the direction of low energy. This is due to the fact that the atomic orbitals of $Sm^{3+}$, $Ti^{4+}$ and $O^{2-}$ form a Ti–O–Sm bridging

**Table 2.** Atomic percentage contents of $TiO_2$ nanotubes and $Sm_2O_3/TiO_2$ nanotubes.

| | Ti 2p (%) | O 1s (%) | Sm 3d (%) |
|---|---|---|---|
| 0.01 mol $l^{-1}$ $Sm_2O_3/TiO_2$ nanotubes | 32.8 | 56.6 | 10.6 |
| 0.02 mol $l^{-1}$ $Sm_2O_3/TiO_2$ nanotubes | 33.0 | 56.0 | 11.0 |
| 0.03 mol $l^{-1}$ $Sm_2O_3/TiO_2$ nanotubes | 31.8 | 56.6 | 11.6 |
| 0.05 mol $l^{-1}$ $Sm_2O_3/TiO_2$ nanotubes | 27.4 | 56.6 | 16.0 |

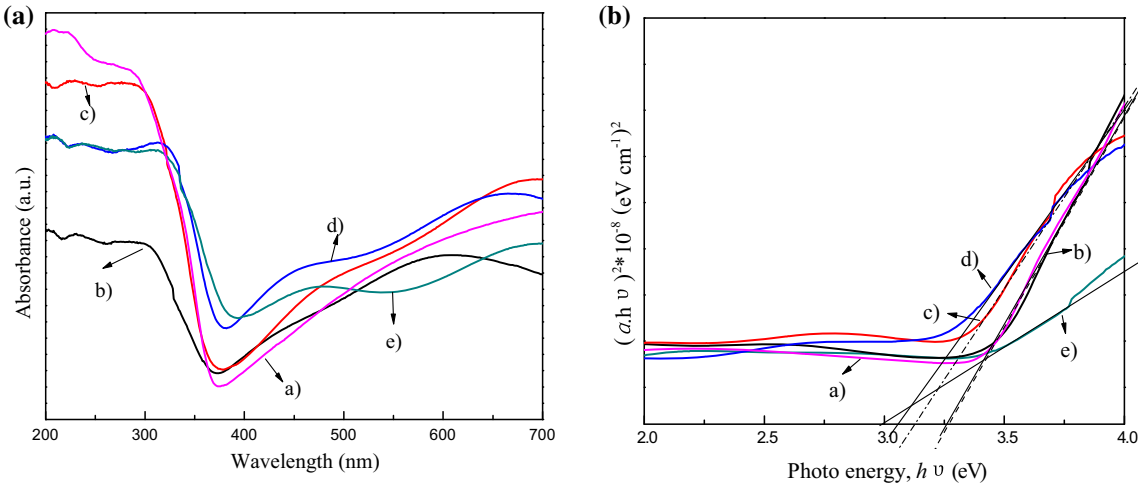


**Figure 4.** (**A**) UV–Vis DRS spectra of $TiO_2$ and Sm-$TiO_2$ nanotubes and (**B**) the plots of $(\alpha h\upsilon)^2$ *vs.* photo energy ($h\upsilon$): (a) $TiO_2$ nanotubes, (b) 0.01, (c) 0.02, (d) 0.03 and (e) 0.05 M Sm–$TiO_2$ nanotubes.

bond. Changing the energy level structure of $TiO_2$ nanotubes can accept the excited electrons in the valence band of $TiO_2$, which can stimulate low-energy photons, trap electrons and reduce the forbidden band width. In the Raman analysis, we know that the grain size of $TiO_2$ is reduced, showing that there are more $Sm^{3+}$ bonding sites on the surface of $TiO_2$ nanotubes. The more bonding sites appear on the surface of $TiO_2$ nanotubes with increase in the concentration of $Sm^{3+}$, resulting in reduction in the band gap.

Figure 5A shows the fluorescence spectroscopy diagram of pure $TiO_2$ nanotube arrays. From the figure, we find that there is a small broad peak at 550 nm, which is originated from an electron radiation recombination of $TiO_2$ nanotube arrays. Since $TiO_2$ is an ionic metal oxide, the valence band is filled with the 2p orbitals of O atom. The conduction band of the lowest energy is composed of the 3d orbital of Ti atom, in which $Ti^{4+}$ is easily oxidized into $Ti^{3+}$, $Ti^{2+}$ and $Ti^{+}$, and local energy levels located within the band gap. The surface state can be used as a fluorescence emission centre to make a weak fluorescence peak of $TiO_2$ nanotube arrays. Figure 5B shows the excitation spectra of different concentrations of Sm–$TiO_2$ nanotubes, in which the emission wavelength set at 613 nm. A strong peak appears at 373 nm, which is attributed to the absorption band gap of $TiO_2$ nanotube arrays, demonstrating the efficient energy transfer from the $TiO_2$ nanotube arrays to $Sm^{3+}$. The weak peak at 410 nm is attributed to the direct excitation of $Sm^{3+}$. Moreover, with an increase in $Sm^{3+}$ concentration, the peak intensity gradually weakenes, which may be due to a high $Sm^{3+}$ content, and more significant absorption of $TiO_2$ nanotube arrays. Figure 5C shows the emission spectra of different concentrations of Sm–$TiO_2$ nanotubes. A combination with the emission spectrum of figure 5B is used to describe the down conversion process. At an excitation wavelength of 370 nm, the emission peak intensity gradually increases with an increase in $Sm^{3+}$ concentration. The maximum emission intensity appears at 0.02 M Sm–$TiO_2$ nanotubes. As the concentration continues to increase, the intensity of the emission peak decreases. This is because $Sm^{3+}$ covers the surface of the $TiO_2$ nanotubes to shorten the distance between $Sm^{3+}$ and $Sm^{3+}$. The $Sm^{3+}$ emission is easily absorbed by adjacent $Sm^{3+}$, resulting in a decrease in peak intensity. The bands of emission at 586, 614 and 667 nm are the electronic transitions of $^4G_{5/2}$–$^6H_{5/2}$, $^4G_{5/2}$–$^6H_{7/2}$ and $^4G_{5/2}$–$^6H_{9/2}$ of $Sm^{3+}$, which is within the absorption range of visible light. It can be seen that the characteristic fluorescence is represented at 370 nm. It suggests that $Sm^{3+}$-modified $TiO_2$ nanotube arrays can convert the absorption of sunlight into visible light absorption. It can increase the utilization of light and electron injection rates of the $TiO_2$ conduction band, which can improve the photocatalytic efficiency.

Although 4f electrons have been shielded by $5s^25p^6$, the spin-coupling constants are relatively large to cause energy level splitting. In crystal field theory, this structure can be split from the $^6H_J$ to 2J + 1 energy levels. The radius of $Sm^{3+}$ is much larger than the radius of $Ti^{4+}$. Therefore, $Sm^{3+}$ cannot replace $Ti^{4+}$ and enter its lattice. Excellent splitting of $^6H_J$ can indicate that $Sm^{3+}$ fits well in a regular environment, and infers that part of $Sm^{3+}$ enters the lattice gap to disturb the octahedral structure of $TiO_6$. According to the model of Frindell *et al* [27], the photoluminescence (PL), process model is plotted in figure 6: (1) The process of excited electrons in the ultraviolet region. (2) The non-radiative energy transfer process for excited electrons to defect states. (3) The non-radiative energy transfer process from the defect state to $Sm^{3+}$. (4) The emission process for $Sm^{3+}$. After addition of $Sm^{3+}$, the fluorescence emission of rare earth comes from the energy transfer from the $TiO_2$ conduction band to $Sm^{3+}$ caused by surface defects of $TiO_2$ nanotube arrays. Jing *et al* [28] considered that the fluorescence emission of $Sm^{3+}$ is indirectly stimulated after electron–hole energy transfer in the

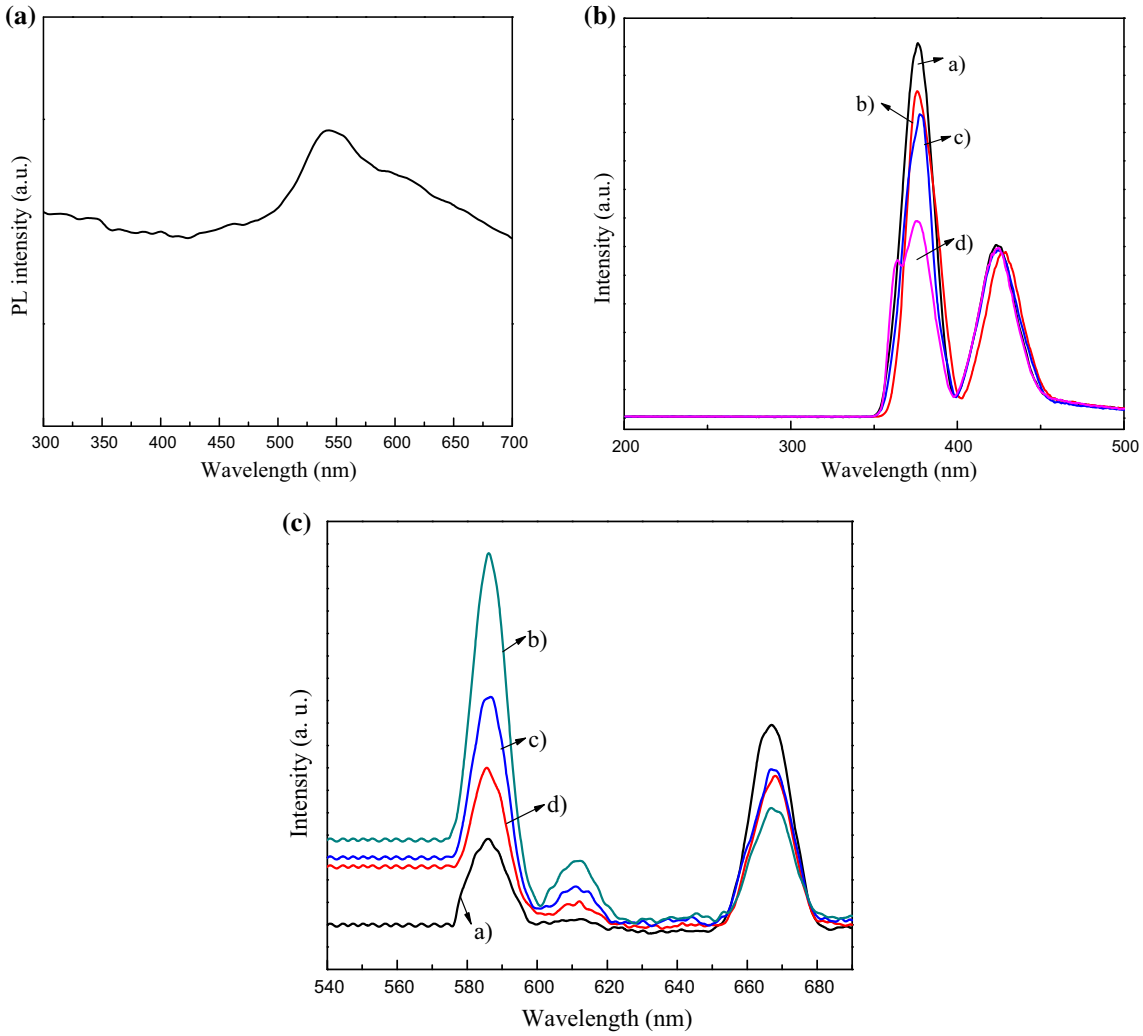


**Figure 5.** (**A**) PL spectra of $TiO_2$ nanotubes; (**B**) the excitation spectra of Sm–$TiO_2$ nanotubes ($\lambda_{em}$ = 613 nm) and (**C**) the emission spectra of Sm–$TiO_2$ nanotubes ($\lambda_{ex}$ = 370 nm): (a) $TiO_2$ nanotubes, (b) 0.01, (c) 0.02, (d) 0.03 and (e) 0.05 M Sm–$TiO_2$ nanotubes.

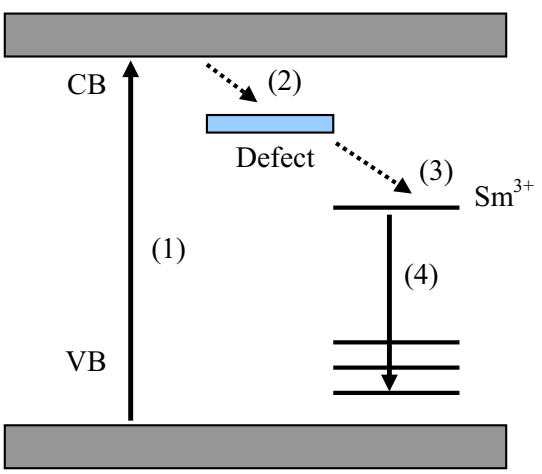


**Figure 6.** Schematic of the PL process of Sm–$TiO_2$ nanotubes.

$TiO_2$ host. They think that energy transfer does not appear on the surface defects, but occurs directly in the internal core energy level of $Sm^{3+}$ to the $^6H_J$ energy level (J = 5/2, 7/2, 9/2 and 11/2). There will be splitting of the emission peak, which is attributed to Stark's energy level splitting due to $Sm^{3+}$ located in a non-cubic crystal field. It can be understood that due to the occurrence of $Sm^{3+}$, the crystal lattice of $TiO_2$ is perturbed, and a non-cubic shape appears. In general, $Sm^{3+}$ has a very good fluorescence spectrum structure in a regular crystal field environment.

Figure 7 shows photocatalytic degradation of the as-prepared $TiO_2$ nanotube arrays and different concentrations of Sm–$TiO_2$ nanotubes, which was determined from the UV–visible spectra at 699 nm. The as-prepared samples were immersed in 100 ml MB solution. All Sm–$TiO_2$ nanotubes were higher than bare $TiO_2$ nanotube arrays. It was observed that within 60 min of degradation, efficiency was about

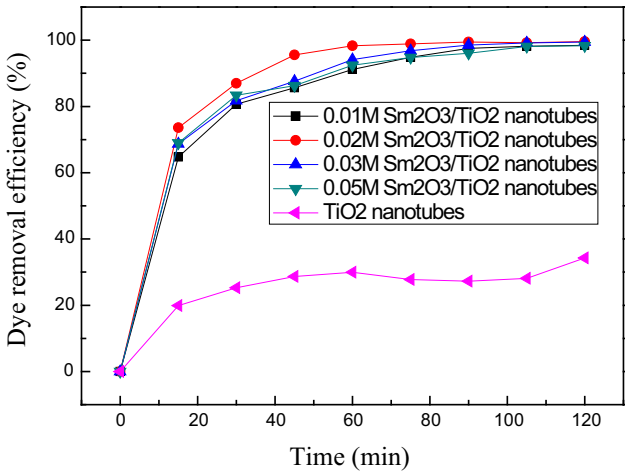


**Figure 7.** Photocatalytic degradation of the as-prepared $TiO_2$ nanotube arrays and Sm–$TiO_2$ nanotubes.

99% for 0.02 M Sm–$TiO_2$ nanotubes, which is much more than twice that of pure nanotubes. Therefore, 60 min was concluded to be the equilibrium time for degradation. With an irradiation time increasing to 120 min, no further enhancement of dye degradation was obtained. The trend of all the samples is the same. In general, the degradation efficiency depends on both the particle size and as well as on the surface area. However, in our work, we may speculate that the photodegradation of organic contaminants mainly depends on visible light utilization and electronic transition. We also discussed the mechanism of photocatalytic performance as shown in figure 6. On the one hand, utilization of visible light depends on the $Sm^{3+}$ modification, which in turn, may help to enhance MB degradation in the aquatic environment used in the present study. On the other hand, we consider that enough surface defects can produce lots of active sites due to addition of $Sm^{3+}$, in which the oxygen vacancies can trap electrons to separate electrons and holes. The electrons life will be extended.

## 4. Conclusion

In summary, the $TiO_2$ nanotube arrays with a vertical tube structure were modified with different concentrations of $Sm^{3+}$ using a simple hydrothermal method, which was used for degradation in organic contaminants and it exhibited excellent performance. The highest efficiency for 0.02 M $Sm^{3+}$ deposited on $TiO_2$ nanotubes can obtain 99% dye degradation, which is much higher than bare $TiO_2$ nanotubes. These results indicate that $Sm^{3+}$ is not only has down-shifting function to increase the light utilization, but it can also be considered as an electron capture zone on the surface of $TiO_2$ nanotubes to extend the electron life.

## Acknowledgements

We would like to express their gratitude to Young reserve talents of Harbin (RC2017QN017002), Heilongjiang Provincial Department of Education Innovative Talent Program (UNPYSCT-2018132) and Harbin university of commerce youth program (18XN027).

## References

[1] Grätzel M and O'Regan B 1991 *Nature* **353** 737
[2] Grätzel M 2001 *Nature* **414** 338
[3] Grätzel M 1995 *Electrochim. Acta* **40** 643
[4] Benkstein K D, Kopidakis N, Lagemaat J V D and Frank A J 2003 *J. Phys. Chem. B* **107** 7759
[5] Charoensirithavorn P, Ogomi Y, Sagawa T, Hayase S and Yoshikawa S 2009 *J. Cryst. Growth* **311** 757
[6] Liu Z Y, Subramania V and Misra M 2009 *J. Phys. Chem. C* **113** 14208
[7] Shen Q, Sato T, Hashimoto M, Chen C C and Toyoda T 2006 *Thin Solid Films* **499** 299
[8] Zhang Q, Wang H, Chen S, Su Y and Quan X 2017 *RSC Adv.* **7** 13223
[9] Mazierski P, Nadolna J, Lisowski W and Winiarski M J 2017 *Catal. Today* **284** 19
[10] Honciuc A, Laurin M and Albu S 2014 *J. Phys. Chem. C* **114** 20146
[11] Lu R, Wang C and Wang X 2018 *Int. J. Nanomed.* **13** 2037
[12] Yu J, Dai G and Huang B 2009 *J. Phys. Chem. C* **113** 16394
[13] Song P, Zhang X, Sun M, Cui X and Lin Y 2012 *Nanoscales* **4** 1880
[14] Hafez H, Wu J H, Lan Z, Li Q H and Xie G X 2010 *Nanotechnology* **21** 415201
[15] Grätzel M 2005 *Inorg. Chem.* **44** 6841
[16] Bingham S and Daoud W A 2011 *J. Mater. Chem.* **21** 2041
[17] Mou P, Pal U, Jiménez J and Pérez-Rodríguez F 2012 *Nanoscale Res. Lett.* **7** 1
[18] Li Q B, Lin J M, Wu J H, Lan Z and Wang Y 2011 *Electrochim. Acta* **56** 4980
[19] Saif M 2009 *J. Photochem. Photobiol. A: Chem.* **205** 145
[20] Yin J B and Zhao X P 2009 *Mater. Chem. Phys.* **114** 561
[21] Gafoor A K A, Thomas J, Musthafa M M and Pradyumnan P P 2011 *J. Electron. Mater.* **40** 2152
[22] Gao C M, Song H W, Hu L Y, Pan G H and Qin R F 2008 *J. Lumin.* **128** 559
[23] Kiisk V, Reedo V, Karbowiak M, Brik M G and Sildos I 2009 *J. Phys. D: Appl. Phys.* **42** 125107
[24] Liu R, Yang W D and Qiang L S 2012 *J. Power Sources* **199** 418
[25] Xu C Y, Zhang P X and Yan L 2001 *J. Raman Specrosc.* **32** 862
[26] Ohsaka T 1980 *J. Phys. Soc. Jpn.* **48** 1661
[27] Frindell K L, Bartl M H and Robinson M R 2003 *J. Solid State Chem.* **172** 81
[28] Jing F L, Harako S and Komuro S 2009 *J. Phys. D: Appl. Phys.* **42** 085109